Disturbance rejection by acceleration feedforward for marine surface vessels

Øivind Kåre Kjerstad and Roger Skjetne

August 15, 2015

Abstract

This paper presents a novel control design architecture for rigid body motion control of marine surface vessels subject to severe rapidly changing exogenous disturbances. Acceleration signals together with actuation feedback are introduced to form a feedforward signal representing the external loads and enable reactive disturbance attenuation in the control law. To handle bias and gravity influence the acceleration measurements these are included in the state estimation problem. The state observer is therefore partly reformulated to use kinematic and sensor models for describing the velocity dynamics. This reduces the model uncertainty. A case study presents findings from experimental data and closed-loop high fidelity simulations of dynamic positioning of a marine vessel in an Arctic offshore operation in managed sea ice.

Feedback control; Feedforward control; State estimation; Disturbance rejection

1 Introduction

In motion control the main objective is typically to control the position and velocity of an object to a desired state. This is usually done by measurements of the position and, sometimes, velocity. Although these systems are proved stable and robust, it is not given that they handle unmodeled dynamics and environmental disturbances well. Any inertial system controlled by state feedback influenced by a disturbance force step will be pushed away from its desired state and must perform unwanted work to reverse the gained motion.

Inertial sensors, including accelerometers, gyroscopes, and magnetometers, are found in a variety of applications such as consumer electronics, vibration sensing of large structures, impact detection, and navigation. Although extensive research on various aspects of the sensor technology exists (see e.g. [38]), care must be taken when using them in closed-loop control, as unwanted effects such as gravitational sensor influence, measurement bias, and noise can be injected into the feedback loop. This paper deals with these challenges and proposes a control system able to exploit acceleration measurements. This will enhance performance when the target system is subject to loads that cannot be accurately described mathematically for control purposes. Emphasis is put on dynamic positioning (DP) of marine vessels, defined according to [14] as automatically maintaining position (fixed location or predetermined track) exclusively through the use of thrusters. These systems are known to struggle when subject to rapidly changing unmeasured and/or unmodeled environmental loads [5, 16].

Although inertial sensors are widely adopted for navigational purposes, the acceleration signals are seldom utilized directly in the control effort calculations. An exception for marine vessels is found in [28], where such signals are used to enhance the state estimation, and introduce an additional acceleration feedback term in the control law responsible for making the system behave more inert. Here, on the other hand, the distinction is that kinematic and sensor models are considered in the state observer, and that the acceleration signal is used to form a measurement of the net external force acting on the system (as previously proposed by the authors in [24] and [22]). This provides a powerful tool for developing robust control systems. The benefit is reactivity to unmodeled dynamics catering for robust performance. An introductory motivating example is given below to explain the main concept of the acceleration-based feedforward.

The main contributions of this paper are the design methodology incorporating an acceleration-based feedforward term in the control law to compensate disturbances and unmodeled dynamics, and experimental verification of the load estimation and the measurement setup showing the feasibility of these proposed methods.

Mathematical notation: In UGS, UGAS, UGES, etc., stands G for Global, S for Stable, U for Uniform, A for Asymptotic, and E for Exponential. Total time derivatives of $x(t)$ are denoted $\dot{x}, \ddot{x}, x^{(3)}, \ldots, x^{(n)}$. The Euclidean vector norm is $|\mathbf{x}|$, the induced matrix 2-norm is denoted $\|\mathbf{A}\|$, while the signal norm is denoted $\|u\| := sup\{|u(t)| : t \geq 0\}$. Stacking several vectors into one is denoted $\text{col}(\mathbf{x}, \mathbf{y}, \ldots) \triangleq \left[\mathbf{x}^\top, \mathbf{y}^\top, \ldots\right]^\top$. The smallest and largest eigenvalues of $\mathbf{A} > 0$ is denoted $\lambda_{\min}(\mathbf{A}) > 0$ and $\lambda_{\max}(\mathbf{A}) > 0$, respectively.

1.1 Motivating example

We consider a scalar mechanical system with unity mass and nonlinear damping,

$$\ddot{x} + \dot{x}^3 = u + d(t), \tag{1}$$

where $(x, \dot{x}, \ddot{x})$ is the position, velocity, and acceleration – all measured quantities, u is a control input force, and $d(t)$ is an external disturbance force. The objective is to control $x(t)$ to accurately track a desired position $x_d(t)$, where $(x_d(t), \dot{x}_d(t), \ddot{x}_d(t))$ are all bounded and available signals. We assume the disturbance is bounded, absolutely continuous, and $\exists d_m > 0$ such that $\left|\dot{d}(t)\right| \leq d_m$ a.a. $t \geq 0$.

Let the control law be divided into a nominal term Γ and a term Δ to compensate the disturbance, that is

$$u = \Gamma(t, e) - \Delta, \tag{2}$$

where $e := \mathrm{col}(x - x_d(t), \dot{x} - \dot{x}_d(t))$. The objective of Γ is to ensure a nominal closed-loop performance that satisfies the specification of the control problem when $d(t) = 0$. To this end we define a Hurwitz matrix

$$A = \begin{bmatrix} 0 & 1 \\ -k_1 & -k_2 \end{bmatrix}, \tag{3}$$

and let $P = P^\top > 0$ satisfy the Lyapunov equation $PA = A^\top P = -qI$ with $q > 0$. Using $k = [k_1, k_2]$, we assign the nominal control law

$$\Gamma(t, e) := -ke + \dot{x}^3 + \ddot{x}_d(t). \tag{4}$$

Differentiating $V_0(e) = e^\top P e$ along the solutions of the closed loop system

$$\dot{e} = Ae + b\left(d(t) - \Delta\right), \tag{5}$$

where $b = \mathrm{col}(0, 1)$, gives

$$\dot{V}_0 = -qe^\top e + 2e^\top P b\left(d(t) - \Delta\right), \tag{6}$$

and it follows for $d(t) - \Delta = 0$ that $\{e = 0\}$ is UGES.

The objective of Δ is to handle the disturbance $d(t)$ and recover the nominal performance as closely as possible. We consider using the acceleration measurement and propose two options.

1.1.1 Direct acceleration feedforward

Assume $a(t) = \ddot{x}(t - \delta)$ is the acceleration measurement for (1), where δ is a small known time delay due to signal processing and communication. Then, by direct feedforward, we assign the signal

$$\Delta(t) := a(t) + \dot{x}(t - \delta)^3 - u(t - \delta), \tag{7}$$

which from (1) implies that $\Delta(t) = d(t - \delta)$. Using $p_M = \lambda_{\max}(P)$ it now follows that

$$\begin{aligned} \dot{V}_0 &\leq -q\left|e\right|^2 + 2p_M\left|e\right|\left|d(t) - d(t - \delta)\right| \\ &\leq -\frac{q}{2}\left|e\right|^2 + \Lambda\delta^2, \end{aligned} \tag{8}$$

where $\Lambda := 2\frac{p_m^2 d_m^2}{q}$, and using the Global Lipschitz property $|d(t) - d(\tau)| \leq d_m |t - \tau|$ (following from absolute continuity of $d(t)$ and boundedness of $\dot{d}(t)$). Letting

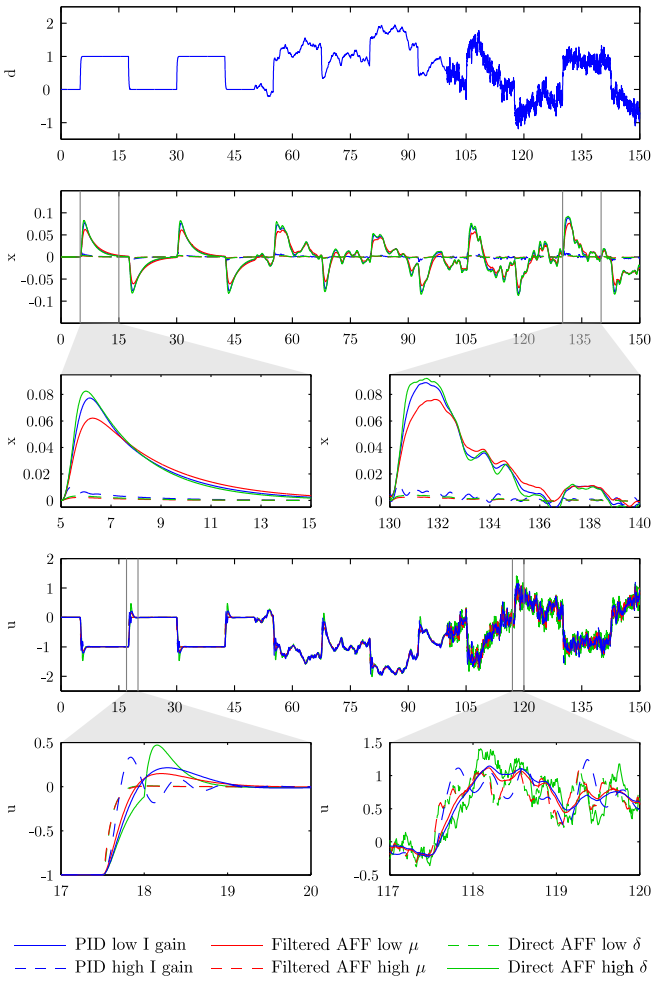

Figure 1: Top: the time development of the state subject to different control strategies. Notice that the disturbance signal is marked by light blue. Bottom: A close-up of the control input.

$\tilde{d}(t) := d(t) - d(t - \delta)$, (8) implies that the resulting closed-loop system

$$\dot{e} = Ae + b\tilde{d}(t) \tag{9}$$

is ISS with respect to $\tilde{d}(t)$ and, correspondingly, the delay δ. A small delay $\delta \ll 1$ will from (8) result in a very small impact by the disturbance on the tracking performance. In the limit as $\delta \to 0$ the difference $\tilde{d}(t)$ vanishes and the nominal performance is recovered.

Note that an alternative to (4) and (7) is to use the simpler control law

$$\begin{aligned} \Gamma(t, e) &:= -ke + \ddot{x}_d(t) \\ \Delta(t) &:= a(t) - u(t - \delta) = d(t - \delta) - \dot{x}(t - \delta)^3, \end{aligned} \tag{10}$$

requiring no measurement of the velocity $\dot{x}$. Instead, the nonlinear damping term is accounted for in the extended disturbance $\bar{d}(t) = d(t) - \dot{x}(t)^3$ such that $\tilde{d}(t) = \bar{d}(t) - \bar{d}(t - \delta)$, and the same conclusion follows.

1.1.2 Filtered acceleration feedforward

We let Δ be the state of a filter to track $d(t)$ as closely as possible. In this case, the control law (2) becomes

dynamic, where $\Gamma(t,e)$ is defined in (4). Letting $\varepsilon := d(t) - \Delta$ be the disturbance tracking error, and differentiating

$$V(e,\varepsilon) = V_0(e) + \frac{1}{2}\varepsilon^2 \tag{11}$$

along the solutions of (5) and $\dot{\Delta}$ gives

$$\dot{V} = -qe^\top e + \left(2e^\top Pb + \dot{d}(t) - \dot{\Delta}\right)\varepsilon. \tag{12}$$

Noticing from (1) and (2) that $\varepsilon = \ddot{x} + \dot{x}^3 - \Gamma(t,e)$, we assign

$$\begin{aligned}\dot{\Delta} &= 2b^\top Pe - \mu\left(\Gamma(t,e) - \ddot{x} - \dot{x}^3\right)\\ &= 2b^\top Pe - \mu\varepsilon.\end{aligned} \tag{13}$$

The derivative of (11) along the solutions of the resulting closed loop system

$$\dot{e} = Ae + b\varepsilon \tag{14}$$

$$\dot{\varepsilon} = -2b^\top Pe - \mu\varepsilon + \dot{d} \tag{15}$$

now becomes

$$\begin{aligned}\dot{V} &= -qe^\top e - \mu\varepsilon^2 + \varepsilon\dot{d}(t)\\ &\leq -q\left|e\right|^2 - \frac{\mu}{2}\left|\varepsilon\right|^2 + \frac{1}{2\mu}\left|\dot{d}(t)\right|^2,\end{aligned} \tag{16}$$

which shows that the system is ISS with respect to $\dot{d}(t)$ as a disturbance input, where the filter gain μ can be used to attenuate its impact on the closed-loop tracking performance.

Note again that we can remove the nonlinear damping term $\dot{x}^3$ from (4) and (13), incorporate it into the extended disturbance $\bar{d}(t) = d(t) - \dot{x}(t)^3$, and arrive at a simpler control law

$$\dot{\Delta} = \left(2b^\top P + \mu k\right)e + \mu\left(\ddot{x} - \ddot{x}_d(t)\right) \tag{17}$$

$$u = -ke - \Delta + \ddot{x}_d(t), \tag{18}$$

which does not need velocity feedback. We notice here that Δ serves as an integral action state on the augmented error $\bar{e} = \mathrm{col}(e,\, \ddot{x} - \ddot{x}_d(t))$.

Figure 1 features x, u, and d from a simulation of (1) where three control laws are compared. Here, $d(t)$ was implemented as disturbance of increasing severity. The compared control laws were:

- A nominal PID control law, $u = -ke - k_i\int e dt$, where $k_i = [k_{i1}, k_{i2}]$ is the integral action gain;
- The direct control law of (4) and (7);
- The filtered control law of (4) and (13).

All of the above were simulated using fixed common nominal control gains $k = [2, 5]$, with low and high disturbance attenuation (k_i, δ, and μ)). For the acceleration feedforward control laws with low disturbance attenuation (high δ and low μ), the performance is comparable to the low gain PID. Increasing the integral action of the PID eventually results in control input oscillations. However, the acceleration feedforward control laws with high disturbance attenuation (low δ and high μ) are able to accurately attenuate the disturbance, recovering the nominal performance, without control input oscillations. Thus, improved control precision is obtained.

2 Problem formulation

For motion control of a rigid-body marine surface vessel we consider the following 3 DOF model,

$$\dot{\eta} = R(\psi)\nu \tag{19a}$$

$$M\dot{\nu} = \tau + \rho(\eta,\nu) + d(t) \tag{19b}$$

where $\eta = \mathrm{col}\,(x, y, \psi) \in \mathbb{R}^3$ is the position and orientation of the body in the inertial frame, $\nu = \mathrm{col}\,(u, v, r) \in \mathbb{R}^3$ is the body-fixed linear and angular velocity of the body, $M = M^\top > 0$ is the rigid body inertia matrix, $\tau \in \mathbb{R}^3$ is the body-fixed control input, $\rho : \mathbb{R}^3 \times \mathbb{R}^3 \to \mathbb{R}^3$ is a locally Lipschitz function containing nonlinear dynamics (Coriolis, damping, and restoring forces), and $d : \mathbb{R}_{\geq 0} \to \mathbb{R}^3$ accounts for external time-varying disturbances. We assume $\exists d_m > 0$ such that $\max\{\|d(t)\|, \left\|\dot{d}(t)\right\|\} \leq d_m$. $R(\psi) \in SO(3)$ is the rotation matrix between the body frame and the inertial frame. This has the following properties,

$$R(\psi)^\top R(\psi) = R(\psi)R(\psi)^\top = I \tag{20}$$

$$\dot{R} = R(\psi)S(r) \tag{21}$$

where $S(r) \in \mathbb{R}^{3\times 3}$ is a skew symmetric matrix with the following properties,

$$S(r) = \begin{bmatrix}0 & -r & 0\\ r & 0 & 0\\ 0 & 0 & 0\end{bmatrix} = -S(r)^\top \tag{22}$$

The objective is to design a control law for the state-of-the-art setup seen in Figure 2 where the acceleration state is applied such that the vessel accurately tracks a predefined time-parameterized trajectory given by $\{\eta_d(t), \nu_d(t), \dot{\nu}_d(t)\}$ while subject to rapidly varying perturbations. Here we consider disturbances arising due to complex unmodeled and unmeasured physical phenomena. Examples include high to extreme sea states, contact with high concentrations of sea ice, tidal currents in shallow water, and operations with interconnection forces between the vessel and equipment or between multiple vessels, amongst others.

Besides the acceleration measurements, which will be treated below, we assume that the following signals are available: The vessel position, $p = \mathrm{col}\,(x, y, z) \in \mathbb{R}^3$, measured in the inertial frame. The vessel orientation, $\Theta = \mathrm{col}\,(\phi, \theta, \psi) \in \mathbb{R}^3$, measured in the body frame relative to the inertial frame. The vessel rate of turn, $\omega = \mathrm{col}\,(p, q, r) \in \mathbb{R}^3$, measured in the body frame relative to the inertial frame. The vessel actuation, $\tau = \mathrm{col}\,(F_x, F_y, M_z) \in \mathbb{R}^3$, measured in the body frame.

Incorporating acceleration measurements for motion control requires the dynamic acceleration vector to be

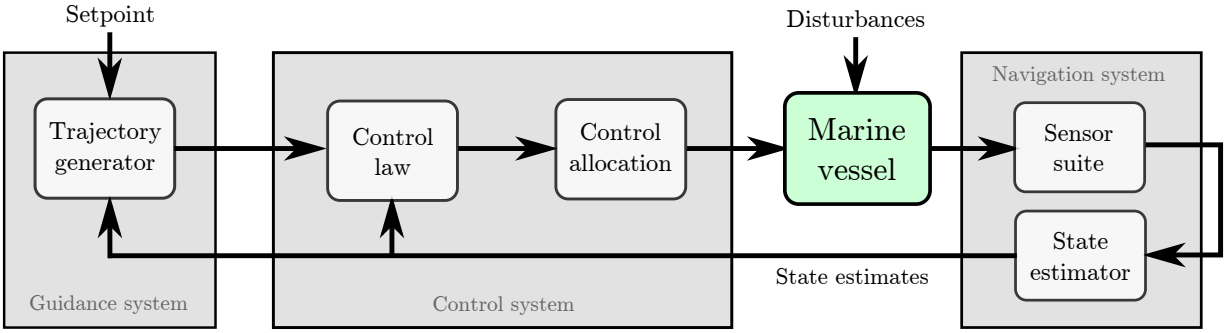

Figure 2: Signal flow in guidance, navigation, and control of marine craft. Adapted from [9].

available. That is the acceleration resulting in motion. This is often regarded as a challenge since accelerometers capture a combination of dynamic acceleration, gravity, and sensor manufacturing/mounting effects such as scale-factor, cross-coupling, and misalignment. Thus the dynamic acceleration must be reconstructed in the navigation system. Here an accelerometer is referred to as a body-fixed three axis orthogonal linear sensor. By assuming that the accelerometer is aligned with the body frame, and that the sensor scale-factor, cross-coupling, and misalignment errors are negligible after calibration, it can be modeled as in [3],

$$a_m = a + \omega \times v + g + b + w \tag{23a}$$
$$\dot{g} = -\omega \times g \tag{23b}$$

where $a_m \in \mathbb{R}^3$ is the sensor output, $a \in \mathbb{R}^3$ is the linear dynamic acceleration in the sensor mounting point, $\omega = \mathrm{col}\,(p, q, r)$ is the angular rate of the body relative to the inertial frame, $v = \mathrm{col}\,(u, v, w)$ is linear velocity of the body. Notice that ν in (19) contains elements of both v and ω. Further, in (23a), $g \in \mathbb{R}^3$ is the gravitational component expressed in the body frame, $b \in \mathbb{R}^3$ is the sensor bias, and $w \in \mathbb{R}^3$ is the sensor noise. Besides acquiring it, there are two main challenges with employing the dynamic acceleration for control of (19). The first is that it may be impractical, or even impossible to mount a sensor in the point of control. This is illustrated in Figure 3 which defines the inertial, body, and sensor frames. Here the point of control will be referred to as CO in the body frame. What arises is a dependency on the distance between CO and the sensor mounting place given by

$$a = a_{\mathrm{co}} + \alpha \times l + \omega \times (\omega \times l) \tag{24}$$

where $a_{\mathrm{co}} \in \mathbb{R}^3$ is the linear dynamic acceleration in CO, $\alpha \in \mathbb{R}^3$ is the angular acceleration, and $l \in \mathbb{R}^3$ is the body frame distance vector between the points of measure and CO. The latter will be referred to as the accelerometer lever arm, or just lever arm.

The second challenge is the fact that a linear sensor does not measure α directly. Here it should be mentioned that sensors capable of measuring α exists [38], but they are not common in marine application. Therefore, such are not considered here. We propose to obtain α through exploiting the lever arm dependency of the accelerometers.

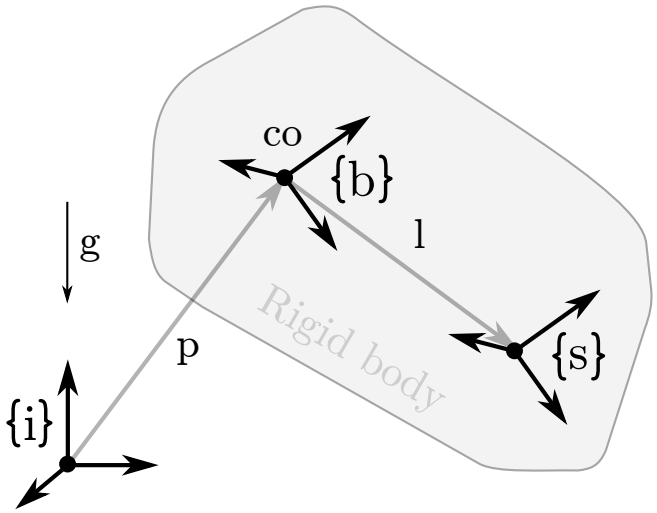

Figure 3: The relation between the inertial frame, the body frame, the point CO, and the point i.

2.1 Problem statement and paper structure

Based on the above statements and assumptions the problem is specified by two subtasks:

1. Design a navigation system that obtains the body-fixed linear and angular acceleration a_{co} and α.

2. Design a reference tracking control law that attenuates the external loads using acceleration feedforward.

The paper is structured as follows. Chapter 3 presents the derivation and verification of an acceleration measurement system, and the design of a state estimation filter capable of estimating a_{co} and α. Chapter 4 derives and analyzes dynamic tracking control laws based on acceleration feedforward. Chapter 5 features a case study investigating dynamic positioning of marine vessels subject to severe disturbances. Finally, Chapter 6 summarizes and concludes the results of the paper.

3 Reconstructing the acceleration state

As mentioned above, it is challenging to measure a_{co} and impossible measure α with one accelerometer. Nevertheless, from (23a) and (24) is can be seen that there is a relation between these and the sensor placement. Therefore we exploit several spatially distributed sensors providing independent measurement equations, and thus enough information to deduce a_{co} and α. This enables use of well known, matured, and relatively cheap and rugged conventional accelerometers in a spatial configuration to setup a virtual 6 DOF accelerometer in CO. Similar schemes are seen in [6] and [37].

Although the control design objective of this paper does not require the 6 DOF acceleration vector, it is practical in both the measurement setup and state estimator to include it.

3.1 6 DOF acceleration measurement

Consider parameterizing (24) as a product of its static and dynamic variables

$$a = \begin{bmatrix} I_{3\times 3} & S(l)^\top & H(l) \end{bmatrix} \begin{bmatrix} a_{\text{co}} \\ \alpha \\ \bar{\omega} \end{bmatrix} \tag{25a}$$

$$= W(l)z. \tag{25b}$$

where $I_{3\times 3} \in \mathbb{R}^{3\times 3}$ is an identity matrix, $S(l)$ is given in (22), and

$$H(l) = \begin{bmatrix} 0 & -l_x & -l_x & l_y & l_z & 0 \\ -l_y & 0 & -l_y & l_x & 0 & l_z \\ -l_z & -l_z & 0 & 0 & l_x & l_y \end{bmatrix}, \tag{26}$$

is a sub-matrix of the accelerometer configuration matrix $W(l) \in \mathbb{R}^{3\times 12}$, and $z \in \mathbb{R}^{12}$ is the linear acceleration, angular acceleration, and angular rate cross product vector. The latter contains $\bar{\omega} \in \mathbb{R}^6$ which is defined as

$$\bar{\omega} = \begin{bmatrix} \omega_x^2 & \omega_y^2 & \omega_z^2 & \omega_x\omega_y & \omega_x\omega_z & \omega_y\omega_z \end{bmatrix}^\top. \tag{27}$$

As mentioned, by measuring in one location $W(l)$ cannot be inverted to find z. Therefore, we propose to use a configuration of four sensors, as illustrated in Figure 4, such that (25b) can be extended to

$$\begin{bmatrix} a_1 \\ a_2 \\ a_3 \\ a_4 \end{bmatrix} = \begin{bmatrix} W(l_1) \\ W(l_2) \\ W(l_3) \\ W(l_4) \end{bmatrix} z \tag{28}$$

$$a_c = G(l_c)z \tag{29}$$

where $G(l_c) \in \mathbb{R}^{12\times 12}$ is the combined sensor configuration matrix and $l_c = \begin{bmatrix} l_1 & l_2 & l_3 & l_4 \end{bmatrix}^\top$ is the combined sensor lever arm vector. To calculate z it is important to ensure that the static matrix $G(l_c)$ is nonsingular. According to [39], this is achieved when the sensors are oriented equally and the measurement positions are not co-planar, i.e. at least one sensor must not lie in the same plane as the others. Then, by substituting in the four accelerometer equations in (23a) for a_c, we get

$$G^{-1} \begin{bmatrix} a_{m1} \\ a_{m2} \\ a_{m3} \\ a_{m4} \end{bmatrix} = z + G^{-1} \begin{bmatrix} \omega \times v + g + b_1 + w_1 \\ \omega \times v + g + b_2 + w_2 \\ \omega \times v + g + b_3 + w_3 \\ \omega \times v + g + b_4 + w_4 \end{bmatrix}. \tag{30}$$

From this it is seen that the setup constitutes a virtual full state accelerometer in CO. Notice that it still has the same sensor effects as (23a) on the measurements.

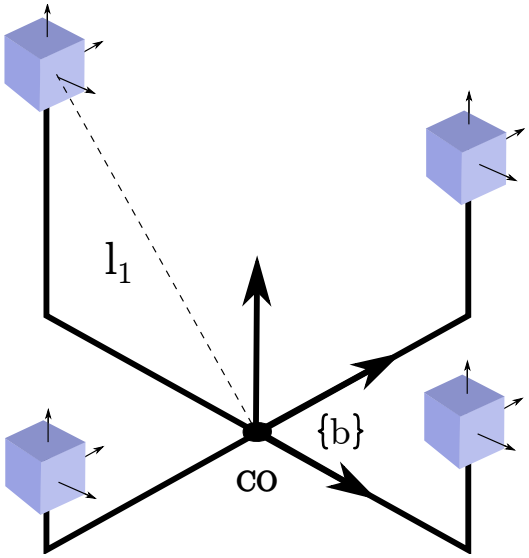

Figure 4: An illustration of one possible setup of the accelerometers for measuring the full state acceleration vector.

MRU 5+

Figure 5: R/V Gunnerus and a MRU 5+. Courtesy of Fredrik Skoglund, and Kongsberg Seatex.

Table 1: Placement of MRUs in R/V Gunnerus relative to CO.

Nr.	X [m]	Y [m]	Z [m]	Note
1	0.358	0.804	-4.321	Technical room
2	14.978	0.039	0.568	Bow bulb
3	-7.454	4.123	-0.012	Engine room stb.
4	-7.545	-4.251	-0.730	Engine room port

3.2 Experimental verification

In November 2013 a series of maneuvering experiments were carried out with the NTNU research vessel Gunnerus offshore mid-Norway. Four Kongsberg Seatex 5+ Motion-Refecence Units (MRUs) [25] were installed onboard. The vessel and sensor are seen in Figure 5. Prior to the campaign, the MRU's lever arms and orientation were accurately measured using laser-based industrial surveying techniques [34]. Table 1 shows the MRU positions.

The MRUs were placed in the vessel hull such that $G(l_c)$ was nonsingular and spatially large. By investigation of the eigenvalues of $G(l_c)^{-1}$ it was found that they were of magnitude less than one. From (30) this implies improved noise and bias attenuation.

Both a and ω were logged from each MRU at 100 Hz by a Kongsberg Seatex Vessel Motion Monitor (VMM). Notice that a, and not a_m was logged. This was due to an proprietary undisclosed algorithm providing the necessary compensation internally in the MRUs.

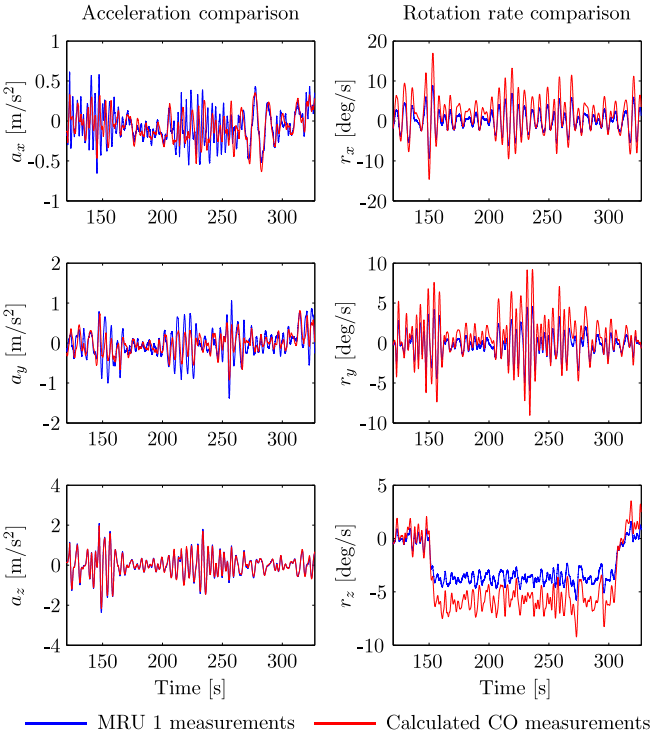

Figure 6: Comparison of the obtained acceleration vector with data output of MRU 1. Left column: The multi-sensor linear accelerations vs. MRU 1 output. Right column: The multi-sensor integration of the angular accelerations vs. MRU 1 gyroscope output.

Figure 6 features the output of the 6 DOF measurement setup compared to MRU 1 data from when Gunnerus performed a turning circle in multi-directional swell waves with significant wave height of 2.1 m and period of 8.5 s. The left column shows the calculated a_{co} compared to MRU 1 a, and the right, $\int \alpha \, dt$ compared to MRU 1 ω.

The results show that the oscillatory wave induced components of the calculated output match well. The deviations in magnitude are believed to stem from the MRU 1 elevated position coupled with roll and pitch motions. In the right column, the angular acceleration is compared to the MRU 1 gyroscope by integration. Although seemingly biased and deviating in magnitude, the oscillatory components of the signals match well, indicating the feasibility of measuring the angular acceleration component.

3.3 State observer

Conventionally, motion control of marine vessels requires a navigation system with an estimator that improves and combines measurements and estimates unmeasured variables (following the structure seen in Figure 2). The objective is to supply the guidance and control systems with necessary motion quantities to calculate trajectories and determine actuation efforts. In DP, a state observer, based on (19) is used [9, 36]. The main limiting factor with such is the precision of the model representing (19b), with respect to the operational environment. The tougher it gets the less precise the estimates become, which in turn results in degraded positioning performance. Incorporating acceleration measurements yields an attractive solution as it contains the net external force directly. If used in a kinematic model it circumvents the need for specific kinetic models.

Here we consider replacing the conventional kinetic model with one that combines kinematic relations together with accelerometer sensor models. This enables estimation of the dynamic acceleration for acceleration feedforward together with the required motion quantities, and can be written as

$$\dot{p}_v = -S(\omega(t))p_v + v \tag{31a}$$
$$\dot{v} = -S(\omega(t))v - b_l - g + B_1 G^{-1} a_{mc} \tag{31b}$$
$$\dot{g} = -S(\omega(t))g \tag{31c}$$
$$\dot{b}_l = 0 \tag{31d}$$
$$\dot{\omega} = b_\omega + B_2 G^{-1} a_{mc} \tag{31e}$$
$$\dot{b}_\omega = 0, \tag{31f}$$

where $p_v := R(\Theta)^\top p$ is the position rotated to the body frame, $v \in \mathbb{R}^3$ is the linear velocity subsystem, $a_{mc} \in \mathbb{R}^{12}$ is the collective accelerometer measurement vector, as seen in (30). $b_l \in \mathbb{R}^3$ and $b_\omega \in \mathbb{R}^3$ are the linear and rotational accelerometer bias originating from the sensor transformation, and $B_{1,2} \in \mathbb{R}^{3\times 12}$ are selection matrices for a_{co} and α, respectively.

The above model is clearly nonlinear as it contains cross products between the states ω and p_v, v, and g, respectively. This must be handled in the state estimator implementation. State of the art for nonlinear systems often implies various nonlinear extensions of the Kalman filter. The downside to this is the lack of established convergence and stability properties. However, in this case a work around is applied. In (31) the objective of the ω state is to remove bias from α. It is assumed that ω is available with high precision and low noise characteristics. Therefore, by regarding it as a time-varying signal

in the position and linear velocity subsystems (31)-(31c) the nonlinear model can be regarded as LTV, and written as,

$$\dot{x} = A(t)x + BG^{-1}a_m \tag{32}$$

$$y = \begin{bmatrix} p_v & \omega \end{bmatrix}^\top \tag{33}$$

where $x = \text{col}(p_v, v, b_l, g, \omega, b_\omega)$. For LTV systems a wide range of Kalman-related results are available; see [17], [10], and [4]. The solution in [2], with the state vector extended by ω and b_ω, is chosen to solve the estimation problem.

Another aspect with (31b) is that it holds two competing integrators in b_l and g. In [3], the subsystem (31a)-(31d) is found uniformly completely observable iff $\omega(t)$ has sufficient perturbations (with $y = p_v$). Although this cannot be guaranteed at all times, it does not constitute a problem as the collective bias $b_l + g$ is uniformly completely observable. Thus, the estimation performance of determining p_v, v, a_{co}, and α is not compromised.

3.3.1 Simulation example

In order to illustrate the behavior of the proposed Kalman filter a simulation of a supply vessel in waves was performed with the open source Marine Systems Simulator [31]. An 82 meter long supply vessel was simulated in 6 DOF with wave loads generated using force response amplitude operators and a JONSWAP spectrum with 10 m significant wave height. A configuration of four distributed accelerometers was used. Besides the lack of measurement noise, these were implemented as described above. The vessel was controlled with a nonlinear PID DP as described in [36]. The estimator bias and gravity initial conditions were set to zero, and at the true value, respectively. Figure 7 feature the resulting state estimate error norms. This indicates the above analytical finding, that the estimation performance of determining p_v, v, a_{co}, and α is not compromised even though the true b_l and g vectors have not been determined. Also, as b_l and g converge the error norms of the remaining estimates are further improved. It should be mentioned that this example implementation is idealistic as it does not tackle the fact that the full characteristics of the sensors with both noise, and different sample rates. Further it does not implement a wave filter, a common component of ship estimators responsible for reducing high oscillatory wave motion on the state estimates.

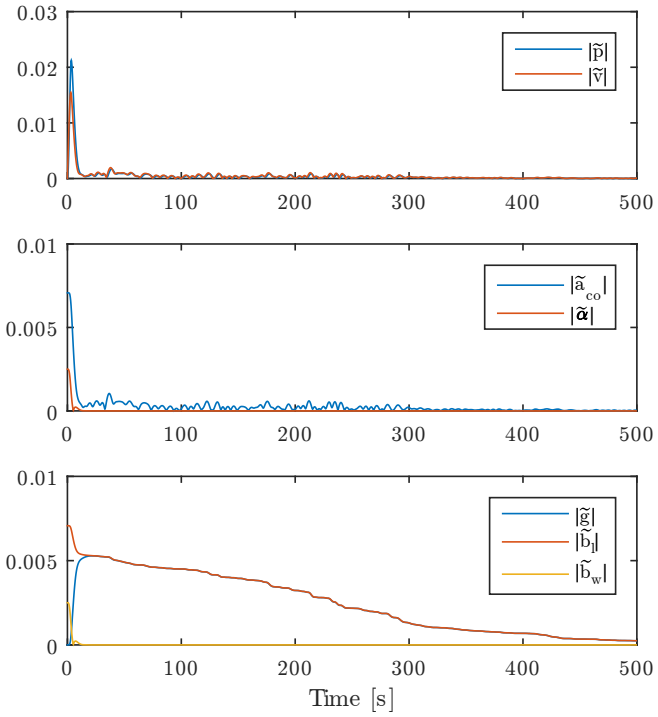

Figure 7: The error norms of the state estimation with the proposed Kalman filter applied to a supply vessel in waves. $\tilde{p} = p - \hat{p}$, $\tilde{v} = v - \hat{v}$, $\tilde{a}_{co} = a_{co} - \hat{a}_{co}$, $\tilde{\alpha} = \alpha - \hat{\alpha}$, $\tilde{g} = g - \hat{g}$, $\tilde{b}_l = b_l - \hat{b}_l$, and $\tilde{b}_w = b_w - \hat{b}_w$, where $\hat{p}$, $\hat{v}$, $\hat{a}_{co}$, $\hat{\alpha}$, $\hat{g}$, $\hat{b}_l$, and $\hat{b}_w$ denotes the state estimates.

4 Control design

In this section we design a control law for (19b) that includes the acceleration signal as a feedforward term to reject the external loads.

Being onboard a ship to be controlled, then you perceive the desired position and position error state relative to the ship pose and not to the NED reference frame. It is therefore convenient to be able to tune the control law with respect to positioning response in the vessel-parallel (VP) frame. Correspondingly, we transform the position/heading vector η from NED to VP, that is, $\eta_v := R(\psi)^\top \eta$.

We define $\eta_{v,d} := R(\psi)^\top \eta_d(t)$, resulting in the VP error state

$$\begin{aligned} \tilde{\eta}_v &= \eta_v - \eta_{v,d} \\ &= R(\psi)^\top (\eta - \eta_d(t)) \\ &= R(\psi)^\top \tilde{\eta}, \end{aligned} \tag{34}$$

where $\tilde{\eta} := \eta - \eta_d(t)$. We similarly define

$$\nu_d := R(\psi)^\top \dot{\eta}_d(t) \tag{35a}$$

$$a_d := \dot{\nu}_d = -S(r)\nu_d + R(\psi)^\top \ddot{\eta}_d(t), \tag{35b}$$

and $\tilde{\nu} := \nu - \nu_d(t)$, where we used $\dot{R} = R(\psi)S(r)$ and $S(r) = -S(r)^\top$. This yields the error dynamics

$$\dot{\tilde{\eta}}_v = -S(r)\tilde{\eta}_v + \tilde{\nu} \tag{36a}$$

$$M\dot{\tilde{\nu}} = \tau + \rho(\eta, \nu) + d(t) - Ma_d. \tag{36b}$$

To achieve disturbance rejection by acceleration feedforward, we propose the following control law

$$\tau = \Gamma - \Delta \tag{37}$$

where $\Gamma : \mathbb{R}_{\geq 0} \times \mathbb{R}^n \times \mathbb{R}^n \to \mathbb{R}^n$ is a nominal control law, and $\Delta \in \mathbb{R}^n$ is a dynamic disturbance attenuation state. Correspondingly, $\varepsilon(t, \Delta) := d(t) - \Delta$ defines a disturbance rejection error signal.

4.1 Nominal tracking design

We consider first the nominal design, where ε is considered a disturbance input from which we want to render the system input-to-state stable (ISS). The design of the term Δ is left for later. The objective is thus to design a nominal control law for Γ that renders the closed-loop system UGES for the case $\varepsilon = 0$ and ISS for $\varepsilon \neq 0$.

A common approach to achieve UGES is to apply a backstepping-based transformation of the state. Accordingly, we define the linear state transformation $z := \mathrm{col}(z_1, z_2)$ with $z_1 := \tilde{\eta}_v$ and $z_2 := \tilde{\nu} + K_1\tilde{\eta}_v$. Defining $\tilde{x} := \mathrm{col}(\tilde{\eta}_v, \tilde{\nu})$, and letting $K_1 = K_1^\top > 0$ and $K_2 = K_2^\top > 0$ be feedback gain matrices, we get the following proposition based on conventional backstepping.

Proposition 4.1. *There exist positive constants k, λ, and γ such that the solutions of the closed-loop system (36) with the control (37) and*

$$\begin{aligned}\Gamma = &- \left[I + K_2K_1 - MK_1S(r)\right]\tilde{\eta}_v \\ &- \left[K_2 + MK_1\right]\tilde{\nu} - \rho(\eta,\nu) + Ma_d, \end{aligned} \tag{38}$$

satisfies the uniform bound

$$|\tilde{x}(t)| \leq \max\left\{k\,|\tilde{x}(t_0)|\,e^{-\lambda(t-t_0)},\ \gamma \sup_{t_0\leq\tau\leq t}\|\varepsilon(\tau)\|\right\}. \tag{39}$$

Proof. The control law (38) can be rewritten in the z-states as

$$\begin{aligned}\Gamma = &- z_1 - K_2z_2 - \rho(\eta,\nu) + Ma_d \\ &- MK_1\left(\tilde{\nu} - S(r)\tilde{\eta}_v\right), \end{aligned} \tag{40}$$

such that the closed-loop system becomes

$$\dot{z}_1 = -S(r)z_1 - K_1z_1 + z_2 \tag{41a}$$
$$M\dot{z}_2 = -z_1 - K_2z_2 + \varepsilon. \tag{41b}$$

Differentiating the Lyapunov function

$$V(z) = \frac{1}{2}z_1^\top z_1 + \frac{1}{2}z_2^\top M z_2 \tag{42}$$

along the solutions of (41), we get

$$\begin{aligned}\dot{V} &= -z_1^\top K_1 z_1 - z_2^\top K_2 z_2 + z_2^\top\varepsilon \\ &\leq -2c_3\,|z|^2 + |z|\,|\varepsilon| \\ &\leq -c_3\,|z|^2, \qquad \forall\,|z| \geq \frac{1}{c_3}\,|\varepsilon| \end{aligned} \tag{43}$$

where $c_3 = \frac{1}{2}\lambda_{\min}(K_1, K_2)$. We also have $c_1\,|z|^2 \leq V(z) \leq c_2\,|z|^2$ where $c_1 = \frac{1}{2}\min\{1, \lambda_{\min}(M)\}$ and $c_2 = \frac{1}{2}\max\{1, \lambda_{\max}(M)\}$. It follows from ISS theorems [20, Theorem 4.6] that the solutions in the z-coordinates satisfy

$$|z(t)| \leq \max\left\{\sqrt{\frac{c_2}{c_1}}\,|z(t_0)|\,e^{-\frac{c_3}{c_2}(t-t_0)},\ \frac{c_2}{c_1c_3}\sup_{t_0\leq\tau\leq t}\|\varepsilon(\tau)\|\right\} \tag{44}$$

The state transformation can be written $z = T\tilde{x}$ where

$$T := \begin{bmatrix} I & 0 \\ K_1 & I \end{bmatrix}, \qquad T^{-1} = \begin{bmatrix} I & 0 \\ -K_1 & I \end{bmatrix}, \tag{45}$$

and

$$T^\top T = \begin{bmatrix} I + K_1^\top K_1 & K_1^\top \\ K_1 & I \end{bmatrix} > 0. \tag{46}$$

Letting $\sigma_1 := \sqrt{\lambda_{\min}(T^\top T)}$ and $\sigma_2 := \sqrt{\lambda_{\max}(T^\top T)}$ gives[1] the equivalence relation

$$\sigma_1\,|\tilde{x}| \leq |z| \leq \sigma_2\,|\tilde{x}|. \tag{47}$$

For the exponential convergence bound in (44) we get

$$|\tilde{x}(t)| \leq \frac{\sigma_2}{\sigma_1}\sqrt{\frac{c_2}{c_1}}\,|\tilde{x}(t_0)|\,e^{-\frac{c_3}{c_2}(t-t_0)}, \tag{48}$$

and for the input bound we get

$$|\tilde{x}(t)| \leq \frac{c_2}{\sigma_1c_1c_3}\sup_{t_0\leq\tau\leq t}\|\varepsilon(\tau)\|. \tag{49}$$

Hence, we take $k = \frac{\sigma_2}{\sigma_1}\sqrt{\frac{c_2}{c_1}}$, $\lambda = \frac{c_3}{c_2}$, and $\gamma = \frac{c_2}{\sigma_1c_1c_3}$. □

A slightly different control law can be derived from LgV-backstepping [1].

Proposition 4.2. *There exist positive constants k, λ, and γ such that the solutions of the closed-loop system (36) with the control (37) and*

$$\begin{aligned}\Gamma = &- \left[K_2K_1 - MK_1S(r)\right]\tilde{\eta}_v - \left[K_2 + MK_1\right]\tilde{\nu} \\ &- \rho(\eta,\nu) + Ma_d, \end{aligned} \tag{50}$$

satisfies the uniform bound (39), where $K_1 = C_1 + \kappa_1 I$ and $K_2 := C_2 + \frac{1}{4\kappa_1}I$ with $C_1 = C_1^\top > 0$, $C_2 = C_2^\top > 0$, and $\kappa_1 > 0$.

Proof. We use $z = \mathrm{col}(z_1, z_2)$, $z = T\tilde{x}$ where T is defined by (45), such that the control law (50) becomes

$$\Gamma = -K_2z_2 - \rho + Ma_d - MK_1\left(\tilde{\nu} - S\tilde{\eta}_v\right), \tag{51}$$

such that the closed-loop system becomes

$$\dot{z}_1 = -S(r)z_1 - K_1z_1 + z_2 \tag{52a}$$
$$M\dot{z}_2 = -K_2z_2 + \varepsilon. \tag{52b}$$

Differentiating the Lyapunov function (42) along the solutions of (52), we get

$$\begin{aligned}\dot{V} &\leq -z_1^\top C_1 z_1 - z_2^\top C_2 z_2 + z_2^\top\varepsilon \\ &\leq -\bar{c}_3\,|z|^2, \qquad \forall\,|z| \geq \frac{1}{\bar{c}_3}\,|\varepsilon| \end{aligned} \tag{53}$$

where $\bar{c}_3 = \frac{1}{2}\lambda_{\min}(C_1, C_2)$. The proof hereafter follows the proof of Proposition 4.1, resulting in the constants $k = \frac{\sigma_2}{\sigma_1}\sqrt{\frac{c_2}{c_1}}$, $\lambda = \frac{\bar{c}_3}{c_2}$, and $\gamma = \frac{c_2}{\sigma_1c_1\bar{c}_3}$. □

[1] Note that σ_1 and σ_2 correspond to the minimum and maximum singular values of $T^\top T$.

Contrary to (41), we notice that the closed-loop system (52) makes out a cascade, where the z_2-subsystem for $\varepsilon = 0$ independently converges exponentially to zero while driving the exponentially stable z_1-subsystem. The disturbance rejection error ε will affect this exponential convergence, where ε is first lowpass-filtered through the z_2-dynamics with steady-state gain K_2^{-1} before affecting the tracking error $z_1 = \tilde{\eta}_v$.

We will next design the disturbance rejection term.

4.2 Closing the loop with disturbance rejection design

While the static part of the control law is given by (37) with either (38) or (50), we will now consider a dynamic design to make the disturbance rejection term Δ track the disturbance $d(t)$ as closely as possible. Towards this end we will apply the 3 DOF acceleration signal vector $a(t) = \dot{\nu}(t) \in \mathbb{R}^3$ as a feedforward signal for disturbance rejection.

By applying (37) with either of the control laws in propositions 4.1 or 4.2, we get the error dynamics

$$\dot{z} = A(r)z + B\varepsilon \tag{54}$$

where $A(r)$ and B are defined from (41) or (52), respectively. Moreover, letting $P := \frac{1}{2}\operatorname{diag}(I, M)$ and $Q := \operatorname{diag}(K_1, K_2)$ for (43) or $Q := \operatorname{diag}(C_1, C_2)$ for (53), then in both cases above we have

$$V(z) = z^\top P z \tag{55}$$

$$\dot{V} \leq -z^\top Q z + 2z^\top PB\varepsilon, \tag{56}$$

and we have shown that the system is UGES for $\varepsilon = 0$ and ISS with linear gain from ε as input.

4.2.1 Direct filtered design

With ε defined above as the disturbance rejection error state, we get

$$\dot{\varepsilon} = -\dot{\Delta} + \dot{d}(t). \tag{57}$$

Noting that

$$\varepsilon = d - \Delta = Ma(t) - \Gamma - \rho(\eta, \nu) \tag{58}$$

is an available feedforward signal due to the acceleration measurement, this gives the immediate choice

$$\dot{\Delta} = \mu\left(Ma(t) - \Gamma - \rho(\eta, \nu)\right) \tag{59a}$$

$$= \mu\varepsilon \tag{59b}$$

$$= -\mu\left(\Delta - d(t)\right) \tag{59c}$$

which results in the closed-loop system (54) and

$$\dot{\varepsilon} = -\mu\varepsilon + \dot{d}(t). \tag{60}$$

Theorem 4.1. *The origin $(z, \varepsilon) = (0, 0)$ of the closed-loop system (54) and (60) is UGES for $\dot{d}(t) = 0$ and ISS with $\dot{d}(t)$ as a bounded input.*

Proof. UGES of the origin for $\dot{d} = 0$ is concluded since the closed-loop error system (54) and (60) is a cascade of two UGES subsystems connected with linear gain [20, Appendix C]. From converse Lyapunov theorems [20] there then exists a quadratic Lyapunov function, which becomes an ISS-Lyapunov function with $\dot{d}$ as input. □

With the disturbance rejection filter (59), Δ will attempt to track $d(t)$ with accuracy dependent on the gain μ. If $\dot{d}(t) = 0$ then Δ will exponentially converge to and track d as a type of integral action. For $\dot{d}$ nonzero there will be a tracking error, tunable by the gain μ; however, the previous section shows that the nominal DP control laws (38) or (50) render the DP closed-loop system robust to this deviation.

Another choice is to define the CLF

$$W(z, \varepsilon) := V(z) + \frac{1}{2\mu}\varepsilon^\top\varepsilon. \tag{61}$$

Taking the total time derivative along (54) and (60) yields

$$\dot{W} \leq -z^\top Q z + \varepsilon^\top\left(\frac{1}{\mu}\dot{d} - \frac{1}{\mu}\dot{\Delta} + 2B^\top Pz\right).$$

Noting that $PB = \frac{1}{2}\operatorname{col}(0, I)$, we assign

$$\dot{\Delta} = \mu\left[Ma(t) - \Gamma - \rho(\eta, \nu) + z_2\right] \tag{62a}$$

$$= \mu\left[\varepsilon + z_2\right] \tag{62b}$$

$$= -\mu\left(\Delta - d(t)\right) + z_2, \tag{62c}$$

which gives

$$\dot{W} \leq -z^\top Q z - \varepsilon^\top\varepsilon + \frac{1}{\mu}\varepsilon^\top\dot{d}. \tag{63}$$

The resulting closed-loop error system becomes (54) and

$$\dot{\varepsilon} = -\mu\varepsilon - \mu z_2 + \dot{d}. \tag{64}$$

Theorem 4.2. *The origin $(z, \varepsilon) = (0, 0)$ of the closed-loop system (54) and (64) is UGES for $\dot{d}(t) = 0$ and ISS with $\dot{d}(t)$ as a bounded input.*

Proof. The conclusion follows from $W(z, \varepsilon)$ being a quadratic ISS-Lyapunov function with $\dot{d}$ as input. □

4.2.2 Filtered design based on a disturbance model

Suppose the disturbance is generated by an exogenous model

$$\dot{\xi} = A_d\xi + E_d w \tag{65a}$$

$$d = C_d\xi \tag{65b}$$

where $\xi \in \mathbb{R}^q$, $q \geq 3$, is the disturbance state, d is the output that affects the DP control system, w is Gaussian white noise, (A_d, E_d, C_d) are linear matrices, and (C_d, A_d) is an observable pair.

Assuming $w = 0$, we design a Luenberger-type disturbance observer

$$\dot{\hat{\xi}} = A_d\hat{\xi} + L_d\varepsilon \tag{66a}$$
$$\Delta = C_d\hat{\xi}, \tag{66b}$$

where the injection signal $\varepsilon = C_d\tilde{\xi} = C_d(\xi - \hat{\xi})$ is generated from (58), and L_d is designed such that $F_d := A_d - LC_d$ is Hurwitz. Correspondingly, let $P_d = P_d^\top > 0$ satisfy $P_dF_d + F_d^\top P_d = -Q_d$. This gives the closed-loop system

$$\dot{z} = A(r)z + BC_d\tilde{\xi} \tag{67a}$$
$$\dot{\tilde{\xi}} = F_d\tilde{\xi}. \tag{67b}$$

Theorem 4.3. *The origin $(z, \tilde{\xi}) = (0, 0)$ of the closed-loop system (67) is UGES.*

Proof. A cascade of two UGES subsystems connected through a linear gain is UGES [20, Appendix C]. □

We note that the disturbance rejection filter (66) can be rewritten as

$$\dot{\hat{\xi}} = F_d\hat{\xi} + L_d d(t) \tag{68a}$$
$$\Delta = C_d\hat{\xi}. \tag{68b}$$

Comparing this to the direct filter design in (59), we recognize $C_d = I$, $L_d = \mu I$, and $A_d = 0$ (such that $F_d = -\mu I$). This indicates that (66) is a general filter that, even if the model (65) is uncertain or unknown, can be designed to improve the filtering performance of the acceleration feedforward-based injection signal ε from (58). However, the more accurately (65) models the disturbance, the better tracking of the disturbance is achieved.

5 DP in ice case study

When vessels designed for Arctic conditions interact with high concentrations of sea ice (above 6/10th surface coverage), the dynamics are substantially different from open water conditions, and conventional open water DP systems are known to be insufficient [11, 13, 16, 19, 21]. However, full-scale, model-scale, and numerical experiments have demonstrated that high-uptime positioning is possible given feasible ice conditions and a reactive DP system [13, 18, 27, 30, 35]. The first is ensured by an icebreaker support fleet which breaks up the incoming natural ice cover and creates a channel of small ice floes for the protected DP vessel to operate in. A reactive DP system can be synthesized by removing the wave filtering and retuning the control system more aggressively. However, since this is based on a simplified open water model lacking the complex and rapidly varying ice dynamics, it will struggle to track and counteract the external loads as these increase. In [32, 33] this problem is alleviated by assuming an accurate ice load measurement. However, practical and reliable measurement systems are not available today. Neither are sufficiently accurate control models capturing the ice dynamics [8, 21]. The reason for this is mainly that the ice loads depend on the in-situ state and properties of the ice floes in direct and indirect contact with the vessel. As the the presented acceleration feedforward methodology avoids the ice load specific measurement and modelling challenges, it is seen as a candidate solution for a reactive system.

Figure 8: The model scale Arctic Drillship during experimental testing at HSVA. Courtesy of DYPIC.

5.1 Preliminaries

This study is divided into two cases. The first investigates a dataset from a model scale DP in managed sea ice experiment performed at the Hamburg Ship Model Basin (HSVA) as a part of the European research and development project DYnamic Positioning in ICe (DYPIC). The project overviews can be can be found in [15, 12]. The second case is a closed-loop numerical simulation using a state-of-the-art high-fidelity numerical program.

For both cases the conceptual and experimentally tested Arctic drillship (ADS) is considered. This was one of two vessels tested during DYPIC, and it is seen in Figure 8. Its main particulars and azimuth thruster arrangement are found in tables 2 and 3. The position and orientation of the vessel in the basin was measured using a Qualisys position reference system. The linear accelerations and rotation rates were measured using an onboard IMU, and the actuation output was measured by load cells in each thruster. All data were logged with 50 Hz. Further description of the ADS is found in [21].

5.2 Case 1: Open-loop disturbance estimation

Model scale trials in ice basins are often used since full scale trials are both impracticality and expensive as it is performed in an uncontrollable environment [7, 16, 26].

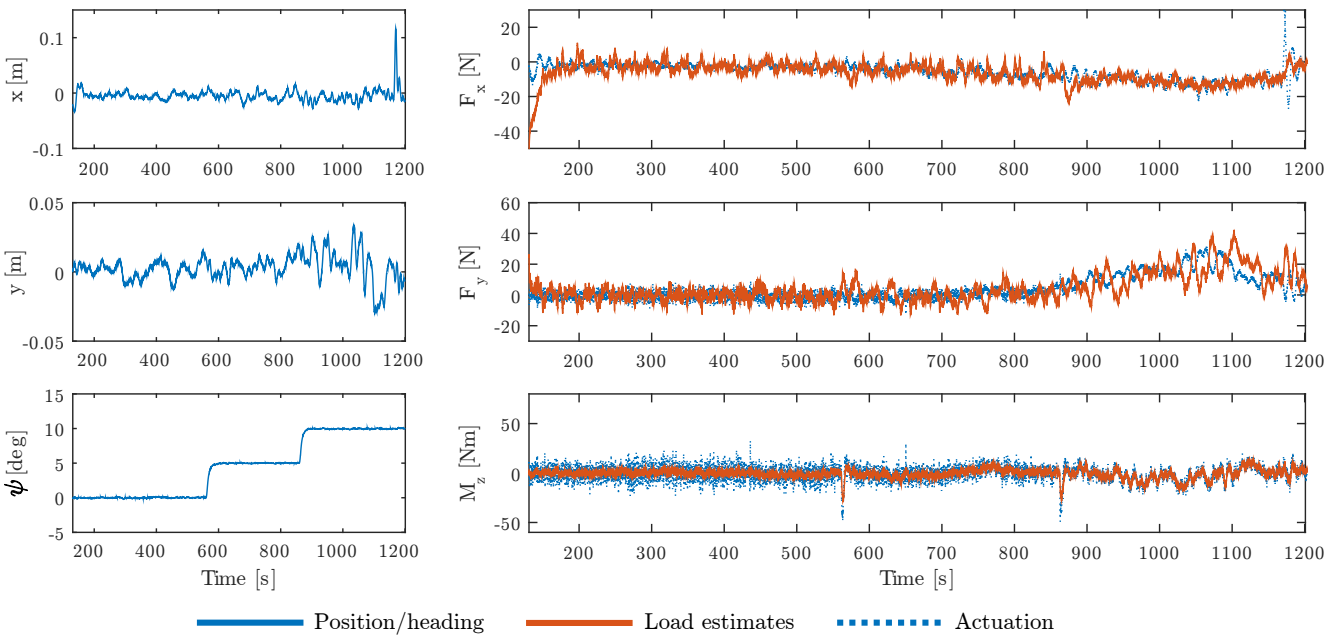

Figure 9: Left: the recorded position and heading of DYPIC experiment 5200 with respect to the moving reference frame. Right: the body frame open-loop disturbance estimates compared to the vessel actuation (in opposite sign for eased interpretation). All data in model scale.

Table 2: The ADS main particulars. FS denotes full scale, MS model scale.

Parameter	FS	MS
Length in design waterline (m)	197.73	6.67
Length between perp. (m)	184	6.13
Breath, moudled (m)	41.33	1.37
Draught at design waterline (m)	12	0.4
Stem angle at design waterline (°)	45	45
Frame angle at midship (°)	45	45
Displacement volume (m^3)	68457	2.535
Centre of gravity from aft. p. (m)	95.34	3.18
Block coefficient	0.75	0.75
Metacentric height (m)	10.71	0.357
Total thrust (N)	$7.2{\cdot}10^6$	270

Table 3: The ADS azimuth thruster arrangement.

No.	Comment	x [mm]	y [mm]	F_{max} [N]
1	Port-Bow	2272	316	45
2	Center-Bow	2644	0	45
3	Stb-Bow	2272	-316	45
4	Center-Stern	-3102	0	45
5	Port-Stern	-2664	190	45
6	Stb-Stern	-2664	-190	45

Table 4: DYPIC experiment 5200 ice field properties.

Property	Value
Ice concentration	70 %
Ice thickness	0.025 m
Min floe size	0.5 x 0.5 m
Max floe size	1.5 x 1.5 m
Ice drift velocity	0.047 m/s

Table 5: DYPIC experiment 5200 DP setpoint segmentation.

No.	Setp. (x [m] ,y [m],ψ [deg])	Length [m]
1.	0, 0, 0°	17
2.	0, 0, 5°	17
3.	0, 0, 10°	17

The foundation for this case is the free floating DP experiment 5200 dataset. This was a free floating DP test where the vessel tracked a reference frame moving with constant velocity through the basin. A commercial ice-adapted DP system controlled the vessel. As the vessel progressed in the basin, the heading setpoint was altered to obtain an oblique angle with respect to the ice drift. It should also be mentioned that the vessel maintained position and heading within allowed tolerances, for all setpoints. However, the ice conditions were relatively mild and the ice concentration then allows the ice floes to be pushed away, rather than broken or rafted by the advancing ship. Key experimental parameters are given in tables 4 and 5. For a more in-depth treatment of the experimental setup, see [21].

As the ADS IMU only contained one accelerometer,

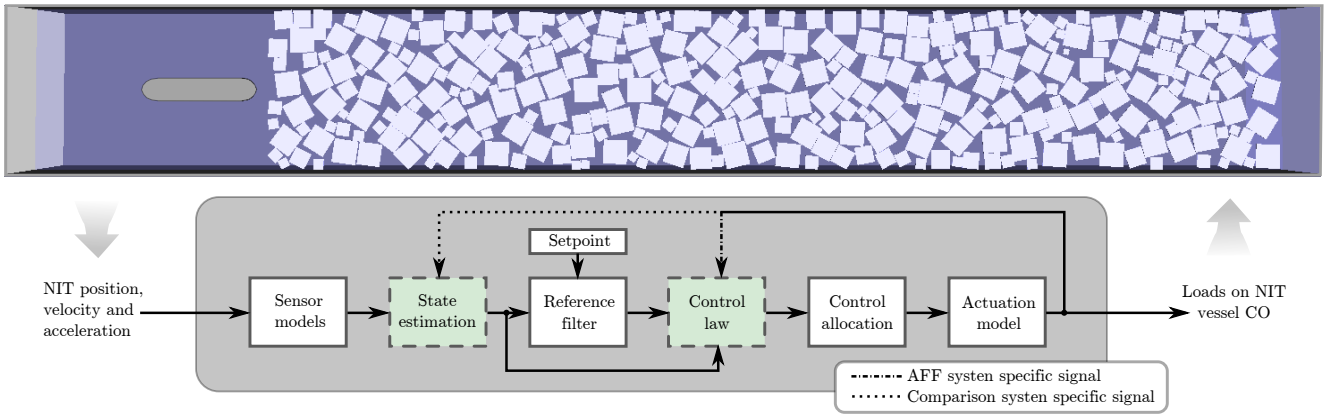

Figure 10: Illustration featuring a rendering from the numerical ice tank indicating the experimental setup, and the overall topology of the simulation program.

the rotational components of the acceleration vector could not be determined. However, the short IMU lever arm together with an experimental setup catering for low rotational rates enables to assume that the measured linear accelerations are close to the ones at CO. Thus, a Kalman filter applying a subset of the model (31a)-(31d) was implemented. To get an idea of the angular acceleration a differentiation of the IMU gyro measurement was performed.

The load estimation was performed using the following filter, derived from (59a) by employing the τ actuation signal and assuming $\rho(\eta, \nu) = 0$,

$$\dot{\Delta} = \mu(Ma(t) - \tau - \Delta) \tag{69}$$

where $\Delta \in \mathbb{R}^3$ is the disturbance estimate, and $\tau \in \mathbb{R}^3$ is the measured actuation vector. For this case study $\mu = 1$ was used.

Figure 9 shows the recorded position and heading of the vessel in the moving reference frame and the planar loads found by the open-loop disturbance estimation compared to the actuation output. It can be seen that the estimates correspond well with the actuation level, but are not identical. This may be attributed to the fact that the vessel experienced perturbations which were not effectively handled by the control system, causing minor deviation from the setpoint (as seen in the position and heading data). These are especially evident towards the end of the experiment in y. Interestingly, the estimates seem to capture the disturbances. The physical explanation for the increase in load and variation is compaction of the ice cover as the vessel advances towards the end of the basin.

The results indicates that the methodology is able to estimate the dynamic acceleration from an accelerometer with the previously mentioned challenges, and calculate the external load including rapidly varying dynamics. However, no definitive verification is possible with this dataset as no independent measurement system was used.

Table 6: Numerical simulation ice conditions.

Parameters	Value	Unit
Water density	1000	kg/m^3
Ice density	900	kg/m^3
Ice flexural strength	45.9	kPa
Ice compressive strength	92	kPa
Ice elastic modulus	10	Mpa
Ice concentration	85	%
Ice thickness	40	mm
Ice drift velocity	0.047	m/s
Max. floe size	1.5	m
Min. floe size	0.5	m

5.3 Case 2: Closed-loop simulation

This study uses the development framework featured in [23]. It closes the loop between a control system and the numerical model of [29], which hereafter will be referred to as the Numerical Ice Tank (NIT). Fig. 10 provides an overview. As the aforementioned references treat both the setup in-depth, only a brief summary is given together with the case setup.

The NIT computes the vessel's dynamics in 6 DOF without wind and waves using a physics engine with tailored routines for ice material modelling. Each simulation is comprised of the following five interconnected elements: the vessel, the towing carriage, the ice floes, the water volume, and the ice tank boundaries. The vessel is simulated as a rigid body in 6 DOF without deformations. The towing carriage is not used in this paper as only free-floating DP mode is considered. The ice floes are simulated as breakable bodies with uniform thickness in 6 DOF. The initial ice floe sizes and floe positions are generated by an ice field generation algorithm that aims to produce a specified ice field. The water is simulated as a static plane that produces buoyancy and drag loads on the vessel and the ice floes. A summary of the considered ice parameters are found in Table 6. These constitute a significantly more challenging scenario than the above experiment.

The motion variables of the vessel in NIT are defined

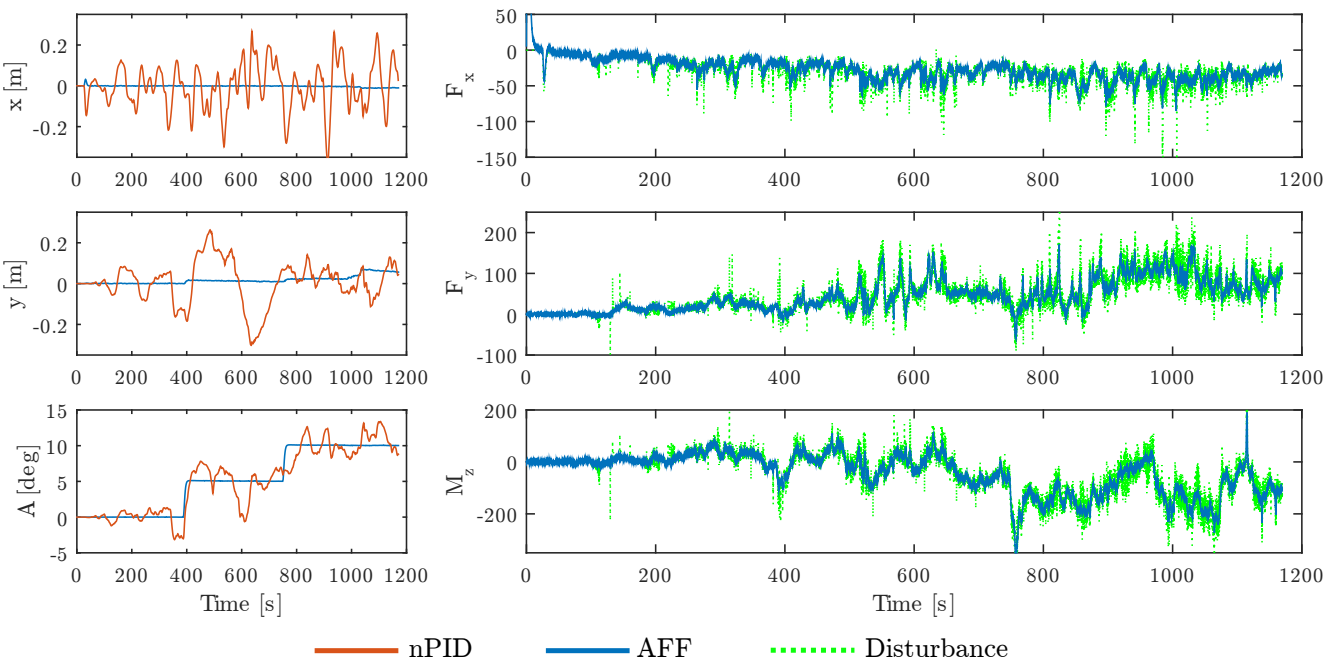

Figure 11: Left: Comparison between ice-adapted nPID and proposed AFF controllers. Right: The estimated disturbance by the rejection filter compared to the simulated disturbance.

Table 7: Placement of accelerometers in the ADS relative to CO for the numerical simulation.

ACC nr.	X [m]	Y [m]	Z [m]	Note
1	3	0	0.3	Bow
2	0	0.6	0	Starboard
3	-3	0	0.3	Stern
4	0	-0.6	0	Port

in three reference frames: *the tank-fixed frame* $\{t\}$ which is non-rotational and fixed to the stationary tank boundaries; *the body frame* $\{b\}$ which is fixed to the vessel; and *the ice floe frames* $\{i\}$ which are fixed to each individual ice floe. Figure 3 illustrates the NIT reference frames. For DP, a fourth reference frame, *the positioning frame* $\{n\}$, is introduced. This is non-rotational and follows a pre-defined trajectory to simulate ice drift in the stationary ice cover. For DP development, {n} is considered inertial, and in this study the DP vessel will be set to track a fixed setpoint in this frame. This approximation is common for simulating ice drift in ice tank testing [12].

The sensor models simulate onboard equipment for measuring the motions of the vessel. They are implemented by first transforming the NIT vessel motion output (i.e. position, orientation, linear velocity, and angular rate) from {t} to {n} and {b}. Then, sensor dynamics and noise are added to the signals. The accelerometers are simulated with both gravity and bias. The actuator models implement the dynamics of the thruster system on-board the vessel. This is approximated with first order dynamics as described in [36].

Two control systems are compared, one acceleration feedforward system with an accelerometer configuration as seen in Table 7, a state observer as described above, the control law of Proposition 4.2, and the direct disturbance rejection filter in (69). For comparison, a state-of-the-art nonlinear PID-type (nPID) control law combined with a nonlinear DP observer, both adapted to ice conditions as described in [23]. In practice this is a more aggressively tuned DP controller where the wave filter has been removed. Two simulations are run with identical ice covers. One for each controller.

The results are shown in Figure 11 where the left column present the position and heading accuracy for the two systems, and the right presents the estimation accuracy of the disturbance rejection filter for the respective simulation. The positioning capabilities show that the acceleration feedforward system outperforms the nPID one. The reason for this is twofold. First, the DP observer is created with the open water model found in [9, 36], without the wave filter. The reason for this is that no dynamical ice models exist. To handle this, all unmodeled dynamics are captured by a bias estimate updated by position measurements, which means that the disturbance must propagate to position/heading response before being captured, creating significant lag. Further increase in injection gains would yield significant oscillations in the estimates. Thus, the state estimates become deteriorated when significantly perturbed. The acceleration feedforward controller does not have this issue, as the external dynamics are captured in the acceleration measurements. Deteriorated state estimates will in turn make the nPID control law produce a inaccurate control output. Also, it relies on integral action to calculate the correct output, but this is not well suited for rapid variations as it is updated by position measurements. Again, the acceleration feedforward system does not have this issue as it tracks the external disturbance

well, as seen in the right column of Figure 11.

6 Conclusions

This paper presented a novel control system design for rigid body motion control subject to severe external disturbances. Acceleration measurements were introduced to capture these dynamics and enable reactive disturbance attenuation. This was done both in the state estimation and control law in an intuitive manner to produce control efforts that counteract rapid variations before they propagate to position and/or heading setpoint deviation, as is the case for systems relying solely on position and heading feedback. The challenge of obtaining a measure of the dynamic acceleration was also addressed with a setup of four accelerometers placed in a specific manner. The proposed design was investigated with both experimental data and high-fidelity simulations, both showing feasibility and the effectiveness of the proposed control setup.

7 Acknowledgments

Research partly funded by the Research Council of Norway (RCN) KMB project no. 199567: Arctic DP, with partners Kongsberg Maritime, Statoil, and DNV GL, and partly by RCN project no. 203471: CRI SAM-CoT. Additionally, the authors would like to thank the MARTEC ERA-NET project: DYPIC - Dynamic positioning in ice covered waters (RCN Project No. 196897), which supplied experimental data from the Hamburg Ship Model Basin, and Mr. Ivan Metrikin for providing the numerical model and great support.

References

[1] Murat Arcak and Petar Kokotović. Redesign of backstepping for robustness against unmodelled dynamics. 11(7):633–643, 2001. Robustness in identification and control.

[2] P. Batista, C. Silvestre, P. Oliveira, and B. Cardeira. Accelerometer calibration and dynamic bias and gravity estimation: Analysis, design, and experimental evaluation. *Control Systems Technology, IEEE Transactions on*, 19(5):1128–1137, 2011.

[3] Pedro Batista, Carlos Silvestre, and Paulo Oliveira. On the observability of linear motion quantities in navigation systems. *Systems & Control Letters*, 60(2):101 – 110, 2011.

[4] Gildas Besançon. Observer design for nonlinear systems. In *Advanced Topics in Control Systems Theory: Lecture Notes from FAP 2005 (Lecture Notes in Control and Information Sciences)*. Springer, 2006.

[5] David Bray. *The DP Operator's Handbook*. The Nautical Institute, 2011.

[6] A. Buhmann, C. Peters, M. Cornils, and Y. Manoli. A GPS aided Full Linear Accelerometer Based Gyroscope-free Navigation System. In *Position, Location, And Navigation Symposium, 2006 IEEE/ION*, pages 622–629, 2006.

[7] D. Deter, W. Doelling, L. Lembke-Jene, and A. Wegener. Stationkeeping in solid drift ice. In *Dynamic Positioning Conference, Houston, Texas, USA*, 2009.

[8] K. J. Eik. *Ice Management in Arctic Offshore Operations and Field Developments*. PhD thesis, Norwegian University of Science and Technology, Trondheim, Norway, 2010.

[9] Thor I. Fossen. *Handbook of Marine Craft Hydrodynamics and Motion Control*. Wiley, 2011.

[10] Jean-Paul Gauthier and Ivan Kupka. *Deterministic Observation Theory and Applications*. Cambridge University Press, 2001.

[11] Arne Gürtner, Bror Henrik Heier Baardson, Glenn-Ole Kaasa, and Erik Lundin. Aspects of importance related to Arctic DP operations. In *Proceedings of the ASME 2012 31st International Conference on Ocean, Offshore and Arctic Engineering OMAE2012, July 1-6, 2012, Rio de Janeiro, Brazil*, 2012.

[12] Andrea Haase and Peter Jochmann. Different ways of modeling ice drift scenarios in basin tests. In *Proceedings of the ASME 2013 32nd International Conference on Ocean, Offshore and Arctic Engineering, June 9-14, 2013, Nantes, France*, 2013.

[13] Torbjørn Hals and Nils Albert Jenssen. DP ice model tests of Arctic drillship and polar research vessel. In *Proceedings of the ASME 2012 31st International Conference on Ocean, Offshore and Arctic Engineering OMAE2012, July 1-6, 2012, Rio de Janeiro, Brazil*, 2012.

[14] International Maritime Organization. *Guidelines for Vessels with Dynamic Positioning Systems*. June 1994. MSC/circ.645.

[15] N. A. Jenssen, T. Hals, A. Haase, X. Santo, S. Kerkeni, O. Doucy, A. Gürtner, S. S. Hetschel, P. O. Moslet, I. Metrikin, and S. Løset. A Multi-National R&D Project on DP Technology in Ice. In *Proceedings of the Dynamic Positioning Conference, Houston, Texas, USA*, 2012.

[16] Nils Albert Jenssen, Suman Muddesitti, Doug Phillips, and Klaus Backstrom. DP In Ice Conditions. In *Dynamic Positioning Conference, Houston, Texas, USA*, 2009.

[17] R. E. Kalman and R. S. Bucy. New results in linear filtering and prediction theory. *Transactions of the ASME. Series D, Journal of Basic Engineering*, 83:95–107, 1961.

[18] Arno Keinonen and Evan H. Martin. Modern day pioneering and its safety in the floating ice offshore. In *Proceedings of the International Conference and Exhibition on Performance of ships and structures in ice*, volume 1, 2012.

[19] S. Kerkeni, X. Dal Santo, and Ivan Metrikin. Dynamic Positioning in Ice - Comparison of Control Laws in Open Water and Ice. In *32nd Int. Conf. Ocean, Offshore and Arctic Engineering (OMAE 2013)*, 2013.

[20] H. K. Khalil. *Nonlinear Control*. Pearson Education Ltd., 2015.

[21] Ø. Kjerstad, I. Metrikin, Sveinung Løset, and Roger Skjetne. Experimental and phenomenological investigation of dynamic positioning in managed ice. *Cold Regions Science and Technology*, 111:67–79, 2015.

[22] Ø. Kjerstad and R. Skjetne. Observer design with disturbance rejection by acceleration feedforward. In *Proceedings of ROCOND12, Aalborg, Denmark*, 2012.

[23] Ø. Kjerstad and R. Skjetne. Modeling and Control for Dynamic Positioned Marine Vessels in Drifting Managed Sea Ice. *Modeling, Identification and Control*, 2014.

[24] Ø. Kjerstad, R. Skjetne, and N. A. Jenssen. Disturbance rejection by acceleration feedforward: Application to dynamic positioning. In *Proceedings of IFAC World Congress, Milan, Italy*, 2011.

[25] Kongsberg Maritime AS. MRU 5+ - The ultimate marine motion sensor. Brochure, 2014.

[26] Walter L. Kuehnlein. Philosophies for Dynamic Positioning in Ice-Covered Waters. In *Proceedings of Offshore Technology Conference, Houston, Texas, USA*, 2009.

[27] Pavel Liferov. Station-keeping in ice - normative requirements and informative solutions. In *Proc. Arctic Technology Conference 2014, Houston, Texas, USA*, 2014.

[28] Karl-Petter W. Lindegaard. *Acceleration Feedback in Dynamic Positioning*. PhD thesis, Norwegian University of Science and Technology, 2003.

[29] I. Metrikin. A Software Framework for Simulating Stationkeeping of a Vessel in Discontinuous Ice. *Modeling, Identification and Control*, 2014.

[30] I. Metrikin, S. Løset, N. A. Jenssen, and S. Kerkeni. Numerical Simulation of Dynamic Positioning in Ice. *Marine Technology Society Journal*, 47(2):14–30, 2013.

[31] MSS. Marine systems simulator, 2010. Viewed 13.04.2014.

[32] D. T. Nguyen, Arild H. Sørbø, and Asgeir J. Sørensen. Modelling and control for dynamic positioned vessels in level ice. In *Proceedings of Conference on Manoeuvring and Control of Marine Craft*, pages 229 – 236, 2009.

[33] Dat H. Nguyen, Dong T. Nguyen, Ser T. Quek, and Asgeir J. Sørensen. Position-moored drilling vessel in level ice by control of riser end angles. *Cold Regions Science and Technology*, 66(2–3):65 – 74, 2011.

[34] Parker Maritime AS. Brochure about Dimensional Control. Brochure, Accessed 2014.

[35] Å. Rohlén. Relationship Between Ice-Management and Station Keeping in Ice. Presentation at Dynamics Positioning Conference, Houston, Texas, USA, 2009.

[36] Asgeir J. Sørensen. *Lecture Notes Marine Cybernetics: Modeling and Control*. Faculty of Engineering Science and Technology, NTNU, Trondheim, Norway, 2005.

[37] Chin-Woo Tan and Sungsu Park. Design of accelerometer-based inertial navigation systems. *Instrumentation and Measurement, IEEE Transactions on*, 54(6):2520–2530, 2005.

[38] D. Titterton and J. Weston. *Strapdown Inertial Navigation Technology, Second Edition (Progress in Astronautics and Aeronautics)*. AIAA, 2005.

[39] B. Zappa, G. Legnani, A. van den Bogert, and R. Adamini. On the Number and Placement of Accelerometers for Angular Velocity and Acceleration Determination. *Transactions of the ASME*, 2001.